

# An Exceptionally Facile Synthesis of Highly Efficient Oxygen Evolution Electrodes for Zinc-Oxygen Batteries

Zhao Yan,<sup>[a, b]</sup> Erdong Wang,<sup>\*[a]</sup> Jianxin Gao,<sup>[a]</sup> Junpeng Yang,<sup>[a, d]</sup> Chuchu Wu,<sup>[a, b]</sup> Luhua Jiang,<sup>[c]</sup> Mingyuan Zhu,<sup>[d]</sup> and Gongquan Sun<sup>\*[a]</sup>

Zinc-oxygen batteries are promising candidates for electrical vehicles and electric grid energy storage due to their low cost, high safety levels, and low environmental impact. The oxygen evolution reaction (OER) and oxygen reduction reaction (ORR) represent the most significant processes in zinc-oxygen batteries. The development of nonprecious metal catalysts for OER with satisfactory performances and low cost (especially prepared by a straightforward synthesis route), still poses a significant challenge. Herein, we report an exceptionally facile and easily scalable method to produce NiFe layered double

hydroxide (LDH) coated nickel foam by immersing nickel foams into aqueous solutions containing NiCl<sub>2</sub> and FeCl<sub>2</sub> and keeping them standing for a certain period of time. Without any other complicated technique or organic reagent, microflower-shaped NiFe LDHs can be obtained. The resulting electrode shows excellent OER performance with a low overpotential of 210 mV at a 10 mA cm<sup>-2</sup> constant current polarization and stable operation for more than 100 charge-discharge cycles in single flow zinc-oxygen batteries.

## 1. Introduction

Recently, with the fast increasing requirement for clean energy and environmental protection, there is an urgent need for economical and efficient energy storage/conversion devices for electric vehicles and electric grid energy storage.<sup>[1]</sup> In recent years, zinc-oxygen batteries, due to their low cost, abundant reserves, good safety and high energy density, have attracted renewed interest as a possible energy storage solution.<sup>[2]</sup> Nevertheless, the application of zinc-oxygen batteries is greatly hampered by the large polarization and low stability of oxygen electrode.

The development of electrocatalysts for oxygen evolution reaction (OER)<sup>[3]</sup> deserves more attention for that the decrease in charge potential not only increase the energy efficiency of zinc-oxygen battery, but also reduce the critical need in stability of electrocatalysts for oxygen reduction reaction (ORR).<sup>[4]</sup> So far, Ir and Ru-based noble-metal catalysts present excellent activity and stability towards OER.<sup>[5]</sup> However, application of these

catalysts is critically restricted due to their scarcity and high cost. Thus, non-precious-metal catalysts attract much attention from scientists and engineers around the world. Layered double hydroxides (LDHs) are a series of layered materials with positively charged metal hydroxide layers and anions in the interlayers to balance excess positive charges.<sup>[6]</sup> LDHs, especially NiFe LDHs, have been reported as the most efficient non-precious catalysts for the OER.<sup>[7]</sup> Lu *et al.*<sup>[8]</sup> electrodeposited NiFe LDHs on nickel foam and achieved 500 mA cm<sup>-2</sup> at 240 mV overpotential. Yang's group<sup>[9]</sup> coupled NiFe LDHs with graphene, which reduced the overpotential of the OER to 206 mV at 10 mA cm<sup>-2</sup>. Nonetheless, fine and complicated synthesis conditions are necessary to prepare LDHs, for example, special and sophisticated facilities were employed in electrochemical synthesis<sup>[8,10]</sup> and pulsed laser ablation,<sup>[11]</sup> high-pressure autoclaves and toxic precipitants, such as urea,<sup>[9,12]</sup> DMF<sup>[13]</sup> or methanol,<sup>[14]</sup> were needed in co-precipitation and hydrothermal methods. All these complex conditions largely limit the practical applications of the LDHs. Hence, exploring new approaches to avoid these drawbacks is highly expected.

Herein, we developed an exceptionally facile hydrolysis-promotion-deposition method (Scheme 1) to produce high

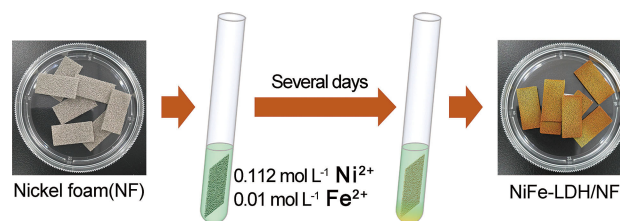
[a] Z. Yan, E. Wang, J. Gao, J. Yang, C. Wu, Prof. G. Sun  
Dalian National Laboratory for Clean Energy, Dalian Institute of Chemical Physics, Chinese Academy of Sciences  
Dalian 116023, China  
E-mail: edwang@dicp.ac.cn  
gqsun@dicp.ac.cn

[b] Z. Yan, C. Wu  
University of Chinese Academy of Sciences  
Beijing 100049, China

[c] L. Jiang  
College of Materials Science and Engineering, Qingdao University of Science and Technology  
Qingdao 266042, China

[d] J. Yang, M. Zhu  
School of Chemistry and Chemical Engineering, Shihezi University  
Shihezi 832003, China

Supporting information for this article is available on the WWW under <https://doi.org/10.1002/celc.201700477>



Scheme 1. The hydrolysis-promotion-deposition method.

efficient NiFe LDHs coated nickel foam oxygen evolution electrodes for zinc-oxygen batteries. Nickel foams were immersed in aqueous solutions containing  $0.112 \text{ mol L}^{-1}$   $\text{NiCl}_2$  and  $0.01 \text{ mol L}^{-1}$   $\text{FeCl}_2$  and kept undisturbed for a certain time (denoted as NiFe-LDH/NF-Xd, X represents the immersing days) to allow the slow hydrolysis of  $\text{Ni}^{2+}$  and  $\text{Fe}^{2+}$ . In this hydrolysis-promotion-deposition method, formation of LDHs is realized due to the following reasons: (i) the extremely low solubility product constants of their corresponding hydroxides allow the precipitation at  $\text{pH} < 7$ ; (ii) the resulting  $\text{H}^+$  from the hydrolysis can be removed by the reaction with nickel foam and oxygen and thus promote the hydrolysis reaction; and (iii) the Fe(II) can be oxidized to Fe(III) to form LDHs by the soluble oxygen in water. The obtained NiFe-LDH/NF electrodes exhibited an ultralow overpotential of 210 mV at  $10 \text{ mA cm}^{-2}$  constant current polarization and perfect stability of over 100 charge/discharge cycles in zinc-oxygen batteries. This method is simple and easily scalable which may reduce the cost of OER electrodes and promote the application of zinc-oxygen batteries.

## 2. Results and Discussion

### 2.1. Characterization of NiFe LDHs

From the electron microscopy images of the NiFe-LDH/NF (Figure 1a–c, S2–4), the NiFe-LDH microflowers consisting of

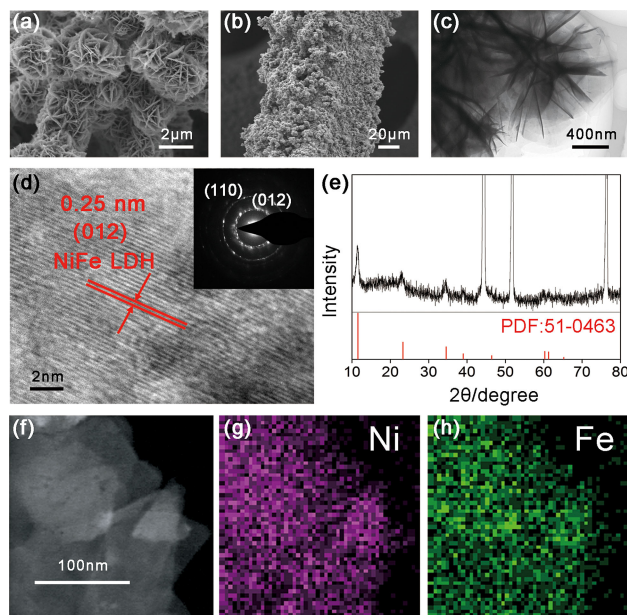


**Figure 1.** Morphology and structural characterizations of NiFe-LDH/NF-15d. a, b) SEM, c) TEM, d) HRTEM images and e) XRD pattern of NiFe-LDH/NF-15d. Inset in (d): SAED image of NiFe-LDH/NF-15d. f–h) Elemental distribution of Ni and Fe in NiFe LDHs.

ultrathin nanoflakes are grown uniformly on the surface of nickel foams. With the increase of the immersing time, more microflowers are appeared, yet no obvious structure change is

observed. High resolution transmission electron microscopy (HRTEM) images in Figure 1d shows that the lattice spacing is 0.25 nm and can be assigned to the (012) plane of NiFe LDHs.<sup>[12–13]</sup> The NiFe-LDH crystal phase (JCPDF: 51-0426)<sup>[6,15]</sup> is also confirmed by the X-ray diffraction (XRD) patterns in Figure 1e and S5. Lattice constants derived from selected area electron diffraction (SAED) images in Figure 1d are consistent with the XRD data (Table S1). Ni and Fe are uniformly distributed on the nanoflakes from the energy dispersive spectrometer (EDS) images in Figure 1f–h. In addition, the results of X-ray photoelectron spectroscopy (XPS) in Figure S6 demonstrate that the binding energy of Ni 2p<sub>3/2</sub> peak centered at 856.3 eV is much higher than that for Ni(OH)<sub>2</sub> at 855.1 eV due to the doped Fe(III) with high-electronegativity.<sup>[16]</sup> All these results reveal the formation of NiFe LDHs with our established facile hydrolysis-promotion-deposition method.

### 2.2. Mechanism of the Formation of NiFe LDHs

To understand the mechanism of the formation of NiFe-LDHs, we tracked the concentrations of Ni and Fe cations in the solution during the preparation process. As shown in Figure 2a,

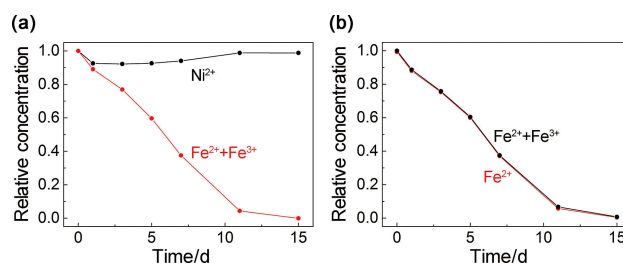


**Figure 2.** Concentration of Ni and Fe cations during the preparation of NiFe-LDH/NF. a) Concentration of Ni and Fe cations measured by inductively coupled plasma-optical emission spectrometry (ICP-OES). b) Concentration of  $\text{Fe}^{2+}$  and total Fe measured by UV/Vis photometry method.

the concentration of Ni decreases a little bit after the beginning of preparation, but regains in the following days. On the other hand, the concentration of Fe decreases nearly linearly with time, and all the Fe is consumed after 15 days.

The concentration of  $\text{Fe}^{2+}$  and  $\text{Fe}^{3+}$  were also distinguished by photometry method with the assistant of 1,10-Phenanthroline, which were displayed in Figure 2b. The trend of the concentration of  $\text{Fe}^{2+}$  is highly consistent with that of total Fe. Moreover,  $\text{Fe}^{2+}$  occupies the absolute majorities of the total Fe along the preparation process. With the above evidences, we propose a potential mechanism of the formation of NiFe LDHs:

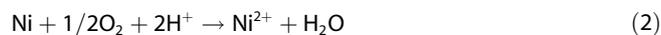
#### (a) Nucleation:

In the first stage,  $\text{Ni}^{2+}$  and  $\text{Fe}^{2+}$  are hydrolyzed to form NiFe-LDH seeds and thus reduce the concentration of Ni and Fe in the solution. It should be noted that  $\text{H}^+$  was produced as a by-product in this procedure [Eq. (1)]:



(b) Reaction promotion:

The formation of  $\text{H}^+$  blocks the precipitation. Fortunately, nickel foam substrate can react with soluble oxygen and  $\text{H}^+$  to promote the precipitation and compensate the concentration of  $\text{Ni}^{2+}$  in the solution [Eq. (2)]. Moreover, the reaction between nickel foam and  $\text{Fe}^{3+}$  can avoid the oxidation of  $\text{Fe}^{2+}$  [Eq. (3)].



(c) Crystal growth:

The crystals of NiFe LDHs are continued to grow with the hydrolysis of  $\text{Ni}^{2+}$  and  $\text{Fe}^{2+}$ . Stage (b) and (c) are occurred simultaneously during the preparation until  $\text{Fe}^{2+}$  is consumed entirely.

(d) Deposition:

Both the nucleation and crystal growth lead to in-situ deposition of NiFe LDHs onto nickel foam substrate.

To confirm this mechanism, comparable experiments and detailed discussion were conducted as follows.

First of all, "Nucleation" and "Crystal growth" stages are driven by the hydrolysis of  $\text{Ni}^{2+}$  and  $\text{Fe}^{2+}$ . To understand the "hydrolysis" process in such a simple aqueous solution, we conducted a series of experiments with different concentrations of  $\text{Ni}^{2+}$  and  $\text{Fe}^{2+}$  with the immersing time of 7 days and listed in Table 1. The precipitation pH of  $\text{Ni}^{2+}$  and  $\text{Fe}^{2+}$  are calculated

**Table 1.** Solution conditions of samples (a–h) prepared by the hydrolysis-promotion-deposition method.

Samples	Concentration [mol L <sup>-1</sup> ]		Precipitation pH		Fe content [%]
	Ni <sup>2+</sup>	Fe <sup>2+</sup>	Ni <sup>2+</sup>	Fe <sup>2+</sup>	
a	0.1	0.005	6.869	6.994	42.1
b	0.112	0.01	6.845	6.844	79.2
c	0.1	0.05	6.869	6.494	96.0
d	0.1	0.1	6.869	6.344	98.8
e	0.005	0.01	7.520	6.844	97.1
f	0.01	0.01	7.369	6.844	96.6
g	0.05	0.01	7.020	6.844	90.1
h	0.5	0.01	6.520	6.844	61.9

by the solubility product constants of their corresponding hydroxides ( $K_{\text{sp}}(\text{Ni}(\text{OH})_2) = 5.48 \times 10^{-16}$ ,  $K_{\text{sp}}(\text{Fe}(\text{OH})_2) = 4.87 \times 10^{-17}$ ).<sup>[17]</sup> It should be noted that the precipitation pH is the initial precipitation condition of a cation and determined by the concentration and solubility product constant. Thus the precipitation pH cannot be changed by adding  $\text{H}^+$  or  $\text{OH}^-$  into the solution (It was discussed in detail in the supporting information). All the OER overpotential values are derived from constant current polarizations for 300s rather than linear sweep voltammetry (LSV) curves to avoid the influence from the overlapped oxidation peak appeared near the onset of oxygen evolution (Figure S7). As shown in Figure 3a and S8, the trend of the OER overpotential curve matches well with the  $\Delta\text{pH}$

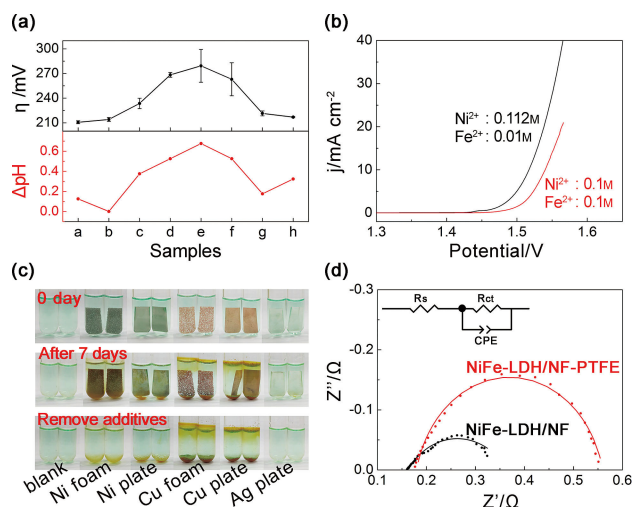


**Figure 3.** a) Overpotential and  $\Delta\text{pH}$  curves of samples a–h. b) LSV curves of samples on GC RDE prepared by the hydrothermal method. c) Photos of preparative solutions with different metal additives. d) EIS curves of NiFe-LDH/NF and NiFe-LDH/NF-PTFE.

curve. The best performance with overpotential of 214 mV is obtained for sample b due to the smallest  $\Delta\text{pH}$  of 0.001. When  $\Delta\text{pH}$  rises to 0.68, the overpotential increases to 279 mV. Homogeneous dispersion<sup>[18]</sup> is extremely required towards excellent OER performance. In our experiments, the NiFe LDHs were obtained from the hydrolysis of precursor cations, thus the simultaneous deposition of  $\text{Ni}^{2+}$  and  $\text{Fe}^{2+}$  is crucial to form a homogeneous precipitation. To meet this end, the concentrations of  $\text{Ni}^{2+}$  and  $\text{Fe}^{2+}$  are tuned aiming at obtain a close precipitation pH. By varying the  $\text{Ni}^{2+}$  and  $\text{Fe}^{2+}$  concentrations as listed in Table 1, nanoflake-like NiFe LDHs can also be formed (Figure S9–11), yet the smaller the  $\Delta\text{pH}$  is, the more uniform the NiFe LDHs deposited on nickel foam. These results prove that homogeneous precipitation can be easily realized by adjusting the concentration of precursors. The atomic fraction of Fe in the precipitates were determined by ICP-OES and listed in Table 1 and S2. The Fe contents follow the same trend as the  $\Delta\text{pH}$  values as well as the overpotentials. In this specific range, the activity decreases with the increase of Fe content due to the electric insulation and chemical instability of  $\text{FeOOH}$ .<sup>[19]</sup> To examine the relationship between precipitation pH and OER performance in widely accepted methods, NiFe LDHs with different concentrations of precursors were also prepared by the hydrothermal method and tested by a glassy carbon rotate disk electrode (GC RDE) with catalyst loading of  $\sim 0.15 \text{ mg cm}^{-2}$ . The 95% iR-corrected LSV curves in Figure 3b and overpotential- $\Delta\text{pH}$  curves in Figure S12 exhibit a similar trend as in Figure 3a. The optimized concentrations of  $\text{Ni}^{2+}$  and  $\text{Fe}^{2+}$  are 0.112 and 0.01 mol L<sup>-1</sup>, which lead to equal precipitation pH and thus low OER overpotential of 286 mV at 10 mA cm<sup>-2</sup>. While 0.1 mol L<sup>-1</sup>  $\text{Ni}^{2+}$  and 0.1 mol L<sup>-1</sup>  $\text{Fe}^{2+}$  are used, the OER overpotential increases to 309 mV. Furthermore, if  $\text{Fe}^{3+}$  is used instead of  $\text{Fe}^{2+}$ , which is common employed in hydrothermal synthesis,<sup>[13,20]</sup>  $\Delta\text{pH}$  can hardly be changed because the concentration ratio of 1016 is needed to get an equal

precipitation pH ( $K_{sp}(\text{Fe}(\text{OH})_3) = 2.79 \times 10^{-39}$ ).<sup>[17]</sup> However, with the hydrolysis-promotion-deposition method, electrodes derived from solution containing  $\text{Ni}^{2+}$  and  $\text{Fe}^{3+}$  also present excellent performance (Figure S13), which can be reasonably explained by that  $\text{Fe}^{3+}$  is able to react with nickel to generate  $\text{Fe}^{2+}$  and then the formation mechanism of the NiFe LDHs follows the one we proposed.

The significance of the “Reaction promotion” process is that it consumes  $\text{H}^+$  by reacting with nickel and oxygen and then promotes the “hydrolysis” process. Oxygen is necessary because nickel cannot react with  $\text{H}^+$  in nearly neutral solution in which the practical redox potential of  $\text{H}_2/\text{H}^+$  is more negative than that of  $\text{Ni}/\text{Ni}^{2+}$ . To confirm this assumption, we conducted control trials with different metal additives. Results in Figure 3c indicate that no observable precipitation was produced in the solution without any metals or with the silver plate. While with the addition of nickel or copper, whether in the form of foams or plates, yellow-brown precipitates are formed due to the consumption of  $\text{H}^+$  by the reaction (2) and (4):



Especially, more precipitates are generated with the existence of copper due to the easier corrosion of copper (Figure S14) and the smaller solubility product constant of the hydrolysis product of copper cations ( $K_{sp}(\text{Cu}(\text{OH})_2) = 2.2 \times 10^{-20}$ ) than  $\text{Ni}(\text{OH})_2$  and  $\text{Fe}(\text{OH})_2$  (Figure S15).

Finally, the “deposition” process in the hydrolysis-promotion-deposition method allows in situ deposition of NiFe LDHs onto nickel foams. This direct deposition process not only enhances the electrical conductivity between NiFe LDHs and nickel foam, which lead to lower resistance and higher activity, but also reinforces the binding force, which leads to higher stability. To understand the relationship between in situ deposition and electrode performance, we coated NiFe LDHs onto nickel foams with PTFE binder (denoted as NiFe-LDH/NF-PTFE, Figure S16) for comparison. The catalyst loading of NiFe-LDH/NF-PTFE was controlled to be the same with the NiFe-LDH/NF-15d (measured by the weight change before and after 15 days immersing), i.e.  $\sim 1.0 \text{ mg cm}^{-2}$ . Figure 3d presents the electrochemical impedance spectroscopy (EIS) of these two electrodes. The NiFe-LDH/NF demonstrates lower internal resistance ( $R_s$ , Table S3) due to the reinforced contact between NiFe LDHs and nickel form substrate.

### 2.3. Electrochemical Performance of NiFe-LDH/NF Electrodes

In order to exploit the potentialities of the hydrolysis-promotion-deposition method, we synthesized NiFe-LDH/NF electrodes with the immersing time range from 6 h to 15 days. For comparison, iridium coated nickel foam (Ir/NF) was prepared by galvanic displacement in  $\text{H}_2\text{IrCl}_6$  with Ir loading of  $1.0 \text{ mg cm}^{-2}$  and tested at the same condition. Figure 4a and S17 plot the overpotential (without iR-compensation) changes with different immersing time. With the increase of immersing time from 6 h to 15 days, the OER overpotential decreases from

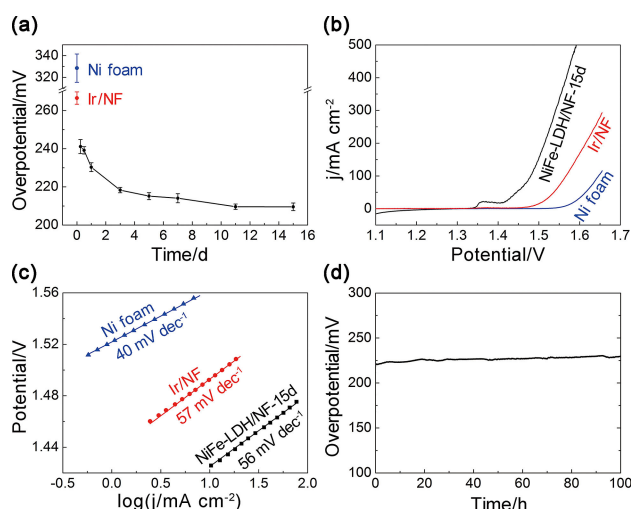


**Figure 4.** a) Overpotential changes of NiFe-LDH/NF versus immersing time at  $10 \text{ mA cm}^{-2}$ ; b) LSV curves and c) Tafel slopes of NiFe-LDH/NF-15d, Ir/NF and Ni foam; d) Durability of NiFe-LDH/NF-15d at  $10 \text{ mA cm}^{-2}$ .

241 mV to 210 mV. The improvement of OER performance with the immersing time can be attributed to two aspects: (i) the increased loading of NiFe LDHs on the nickel foam, (ii) the unique 3D structure of the secondary nanoflakes grown on the primary structure. All these changes lead to an increment in the active surface area, which is confirmed by the SEM images and the Brunauer–Emmett–Teller (BET) data in Figure S2 and S18. As to the Ir/NF and the nickel foam, the OER overpotentials are 266 and 328 mV, respectively, which are much inferior to that of NiFe-LDH/NF electrode. The LSV curves of NiFe-LDH/NF-15d, Ir/NF and nickel foam are displayed in Figure 4b. The oxidation peak at around 1.36 V versus Reversible Hydrogen Electrode (RHE) can be assigned as the redox couple of  $\text{Ni}(\text{II})/\text{Ni}(\text{IV})$ . The NiFe-LDH/NF-15d affords a small onset potential of  $\sim 1.39 \text{ V}$  vs. RHE and provides a current density of  $50 \text{ mA cm}^{-2}$  at  $\sim 1.44 \text{ V}$ . On contrast, the Ir/NF and nickel foam need  $\sim 1.53 \text{ V}$  and  $\sim 1.61 \text{ V}$  to boost the current density of  $50 \text{ mA cm}^{-2}$ , respectively. The Tafel slopes (Figure 4c) of NiFe-LDH/NF-15d and Ir/NF are 56 and  $57 \text{ mV dec}^{-1}$ , which means the electrocatalytic kinetics for OER are similar within these two catalysts.

Besides the high OER activity, the NiFe-LDH/NF-15d exhibits perfect stability in  $1 \text{ mol L}^{-1}$  and  $8 \text{ mol L}^{-1}$  KOH electrolyte (Figure 4d and S19). When applied a constant current density of  $10 \text{ mA cm}^{-2}$  in  $1 \text{ mol L}^{-1}$  KOH, the NiFe-LDH/NF-15d electrode has a relatively stable overpotential of  $\sim 227 \text{ mV}$ . After the 100 h test, the overpotential increases from 210 to 230 mV. The morphology of NiFe-LDH/NF-15d after constant current polarization was characterized and shown in Figure S20. Though the nanoflakes are broken into much smaller pieces, the NiFe LDHs are still uniformly dispersed, which contributes to the stable performance towards OER.

On the basis of the promising activity and stability of the as-prepared NiFe-LDH/NF electrodes, single flow three-electrode zinc-oxygen batteries (Figure 5a) was integrated to investigate the performance of OER electrode in actual working condition. Since the zinc-oxygen batteries were fabricated with

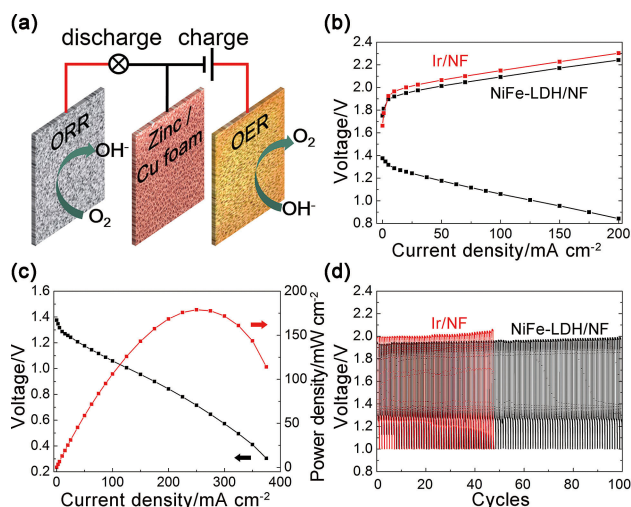


**Figure 5.** Electrochemical performance of a single flow zinc-oxygen battery. a) Schematic of the rechargeable Zn-oxygen battery. b) Charge and discharge polarization curves of Zn-oxygen batteries with different OER electrodes. c) Discharge polarization curves and corresponding power density plots. d) Charge-discharge cycling performance of rechargeable Zn-oxygen batteries at a constant charge-discharge current density of  $20 \text{ mA cm}^{-2}$ .

identical components except for the OER electrodes, charge process was emphasized in our following discussion. As shown in Figure 5b, the zinc-oxygen battery with NiFe-LDH/NF electrode exhibits a lower polarization in the charge process compared to that of Ir/NF electrode. While in the discharge process, the maximum power density of the single flow zinc-oxygen battery reaches  $178 \text{ mW cm}^{-2}$  (Figure 5c), which indicates a high discharge ability of the single flow zinc-oxygen batteries. Figure 5d shows the charge-discharge cycles (charge for 30 min and discharge to  $1.0 \text{ V}$  at  $20 \text{ mA cm}^{-2}$ ) of these two batteries. Obviously, the battery with NiFe-LDH/NF electrode provides smaller charge voltage and much stable cycles. The charge voltage of NiFe-LDH/NF increases to  $1.98 \text{ V}$  at the end of 100 charge-discharge cycles, while charge voltage of Ir/NF raises to  $2.06 \text{ V}$  after 47 cycles. The average energy efficiency of NiFe-LDH/NF based zinc-oxygen batteries reaches  $61.5\%$ , which is larger than that of Ir/NF. The superior activity and stability of NiFe-LDH/NF in zinc-oxygen battery are highly consistent with that in electrochemical measurement, which confirms the advancement of the NiFe-LDH/NF electrodes in actual conditions.

### 3. Conclusions

In summary, NiFe LDHs are successfully synthesized using the hydrolysis-promotion-deposition method. By immersing the nickel foam into solution containing  $0.112 \text{ mol L}^{-1} \text{ Ni}^{2+}$  and  $0.01 \text{ mol L}^{-1} \text{ Fe}^{2+}$ , the formation of NiFe LDHs undergo four steps: (i) in the nucleation step, the metal cations,  $\text{Ni}^{2+}$  and  $\text{Fe}^{2+}$  are hydrolyzed in the aqueous solution, (ii) the nickel foam reacts with the soluble oxygen and  $\text{H}^+$  and promotes the hydrolysis, (iii) the crystals of NiFe LDHs are continued to grow

with the hydrolysis of  $\text{Ni}^{2+}$  and  $\text{Fe}^{2+}$ , (iv) LDHs are formed and deposited in situ onto the nickel foam substrates. With facile controlling the concentration and precipitation pH, Ni and Fe disperse uniformly in the NiFe LDHs. After 15 days' standing in the  $\text{Ni}^{2+}/\text{Fe}^{2+}$  containing solution, the obtained NiFe-LDH/NF-15d exhibits excellent performance towards the OER with an overpotential of  $210 \text{ mV}$  at  $10 \text{ mA cm}^{-2}$ . The electrode is stable with only  $9.5\%$  increment in OER overpotential after the 100 h test and also shows remarkable stability of 100 charge-discharge cycles in zinc-oxygen batteries. The developed hydrolysis-promotion-deposition method provides a brand-new and facile way to manufacture high-performance but low-cost OER electrodes ( $\$24 \text{ m}^{-2}$ , as estimated in Figure S21), and may promote the application of rechargeable zinc-oxygen batteries.

## Experimental Section

### Materials

The nickel foams ( $32 \text{ mg cm}^{-2}$ , thickness:  $1.7 \text{ mm}$ , Tianyu Technology, Heze) were ultrasonicated in acetone and  $1 \text{ mol L}^{-1} \text{ HCl}$  for  $15 \text{ min}$ , respectively, and rinsed with water before use. All other chemicals used in this study, such as  $\text{FeCl}_2 \cdot 4\text{H}_2\text{O}$ ,  $\text{NiCl}_2 \cdot 6\text{H}_2\text{O}$  and  $\text{KOH}$ , were of analytical grade and used as received without further purification.

### Synthesis of NiFe-LDH/NF

In a typical synthesis process,  $3 \text{ mL}$  aqueous solution containing  $0.112 \text{ mol L}^{-1} \text{ NiCl}_2$  and  $0.01 \text{ mol L}^{-1} \text{ FeCl}_2$  was added into a test tube. A piece of nickel foam with the size of  $1 \text{ cm} \times 2 \text{ cm}$  was immersed in the solution. After keeping undisturbed for  $15 \text{ days}$  or a certain time as indicated, the nickel foam was taken out and washed with abundant water. In each condition, seven or more samples were prepared among which five were used to test the OER performance and the others were used in the physical characterization. Thus, the OER performance was the average of these five samples and the deviation was also plotted in the figures.

### Physical Characterization

The morphology of NiFe-LDH/NF were examined by JSM-7800F scanning electron microscope (SEM). Fine structure and element mapping were characterized by Tecnai G2 F20 transmission electron microscope (TEM). Surface composition and valence state were tested by Thermo escalab 250Xi X-ray photoelectron spectrometer (XPS). X-ray diffraction (XRD) patterns of the samples prepared at different conditions were conducted on X'pert Pro (PANalytical,  $60 \text{ kV}$ ,  $55 \text{ mA}$ ) diffractometer using  $\text{Cu K}\alpha$  radiation at a scanning rate of  $5 \text{ min}^{-1}$ . Element composition and concentration were determined by inductively coupled plasma-optical emission spectrometer (ICP-OES, PerkinElmer 7300DV), UV-Vis photometer (UV-2550) and ARL QUANT'X energy-dispersive X-ray fluorescence spectrometer (XRF, Thermo Scientific). Brunauer-Emmett-Teller (BET) data were collected on NOVA 2200e surface area & pore size analyzer (Quantachrome).

## Electrochemical Measurements

Electrochemical measurements were carried out in traditional three-electrode cell, in which NiFe-LDH/NF with an effective projected area of 1 cm<sup>2</sup> was used as the working electrode, Platinum plate as the counter electrode and a double-salt-bridge saturated calomel electrode (SCE) as the reference electrode in 1 mol L<sup>-1</sup> KOH electrolyte. In this paper, all potentials were referred to the reversible hydrogen electrode (RHE). The electrochemical experiments were carried out by using SI 1287A electrochemical interface and SI 1260 impedance/gain-phase analyzer (Solartron Analytical). All these electrochemical experiments were conducted with a water bath at 25 ± 2 °C.

Zinc-oxygen battery were fabricated with a piece of copper foam (2cm × 2cm), a commercial available air electrode (MetAir®, QuantumSphere) and NiFe-LDH/NF as the zinc, ORR and OER electrodes, respectively. Aqueous solution of 8 mol L<sup>-1</sup> KOH with the additive of 0.7 mol L<sup>-1</sup> ZnO was used as electrolyte. The ORR electrode was fed by oxygen at a flow rate of 50 sccm under atmospheric pressure.

## Acknowledgements

The authors acknowledge financial support from the Key Program of the Chinese Academy of Sciences (Grant No. KGZD-EW-T08), the Strategic Priority Research Program of the Chinese Academy of Sciences (Grant No. XDA09030104) and the Youth Innovation Promotion Association of the Chinese Academy of Sciences.

## Conflict of Interest

The authors declare no conflict of interest.

**Keywords:** Electrocatalysis · layered double hydroxide · oxygen evolution reaction · synthetic methods · zinc-oxygen batteries

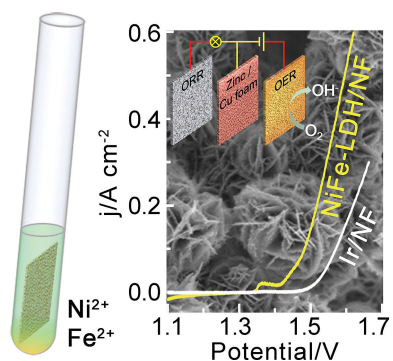
- [1] a) D. Kundu, B. D. Adams, V. Duffort, S. H. Vajargah, L. F. Nazar, *Nat. Energy* **2016**, *1*, 16119; b) J. F. Parker, C. N. Chervin, E. S. Nelson, D. R. Rolison, J. W. Long, *Energy Environ. Sci.* **2014**, *7*, 1117–1124.  
 [2] a) Z. Yan, E. Wang, L. Jiang, G. Sun, *RSC Adv.* **2015**, *5*, 83781–83787; b) A. L. Zhu, D. Duch, G. A. Roberts, S. X. X. Li, H. Wang, K. Duch, E. Bae, K. S. Jung, D. Wilkinson, S. A. Kulinich *ChemElectroChem* **2015**, *2*, 134–142; c) M. Wang, T. Qian, J. Zhou, C. Yan, *ACS Appl. Mater. Interfaces* **2017**, *9*, 5213–5221; d) S. S. Shinde, C.-H. Lee, A. Sami, D.-H. Kim, S.-U. Lee, J.-H. Lee, *ACS Nano* **2017**, *11*, 347–357; e) A. L. Zhu, D. P. Wilkinson, X. Zhang, Y. Xing, A. G. Rozhin, S. A. Kulinich, *Journal of Energy Storage* **2016**, *8*, 35–50.  
 [3] a) F. Dionigi, P. Strasser, *Adv. Energy Mater.* **2016**, *6*, 1600621; b) S. Klaus, L. Trotochaud, M.-J. Cheng, M. Head-Gordon, A. T. Bell, *ChemElectro-*

- Chem* **2016**, *3*, 66–73; c) J. A. Haber, C. Xiang, D. Guevarra, S. Jung, J. Jin, J. M. Gregoire, *ChemElectroChem* **2014**, *1*, 524–528; d) N.-T. Suen, S.-F. Hung, Q. Quan, N. Zhang, Y.-J. Xu, H. M. Chen, *Chem. Soc. Rev.* **2017**, *46*, 337–365.  
 [4] a) J. Yang, J. Hu, M. Weng, R. Tan, L. Tian, J. Yang, J. Amine, J. Zheng, H. Chen, F. Pan, *ACS Appl. Mater. Interfaces* **2017**, *9*, 4587–4596; b) Z. Zhang, H. Li, J. Hu, B. Liu, Q. Zhang, C. Fernandez, Q. Peng, *J. Alloys Compd.* **2017**, *694*, 419–428.  
 [5] a) J. Suntivich, K. J. May, H. A. Gasteiger, J. B. Goodenough, Y. Shao-Horn, *Science* **2011**, *334*, 1383–1385; b) Y. Lee, J. Suntivich, K. J. May, E. E. Perry, Y. Shao-Horn, *J. Phys. Chem. Lett.* **2012**, *3*, 399–404; c) P. Tan, Z. H. Wei, W. Shyy, T. S. Zhao, X. B. Zhu, *Energy Environ. Sci.* **2016**, *9*, 1783–1793; d) T. Audichon, S. Morisset, T. W. Napporn, K. B. Kokoh, C. Comminges, C. Morais, *ChemElectroChem* **2015**, *2*, 1128–1137; e) K. S. Exner, J. Anton, T. Jacob, H. Over, *ChemElectroChem* **2015**, *2*, 707–713.  
 [6] L. Qian, Z. Y. Lu, T. H. Xu, X. C. Wu, Y. Tian, Y. P. Li, Z. Y. Huo, X. M. Sun, X. Duan, *Adv. Energy Mater.* **2015**, *5*, 1500245.  
 [7] a) C. N. Chervin, P. A. DeSario, J. F. Parker, E. S. Nelson, B. W. Miller, D. R. Rolison, J. W. Long, *ChemElectroChem* **2016**, *3*, 1369–1375; b) B. Weng, F. Xu, C. Wang, W. Meng, C. R. Grice, Y. Yan, *Energy Environ. Sci.* **2017**, *10*, 121–128.  
 [8] X. Lu, C. Zhao, *Nat. Commun.* **2015**, *6*, 6616.  
 [9] X. Long, J. Li, S. Xiao, K. Yan, Z. Wang, H. Chen, S. Yang, *Angew. Chem. Int. Ed.* **2014**, *53*, 7584–7588.  
 [10] F. Y. Ning, M. F. Shao, S. M. Xu, Y. Fu, R. K. Zhang, M. Wei, D. G. Evans, X. Duan, *Energy Environ. Sci.* **2016**, *9*, 2633–2643.  
 [11] a) B. M. Hunter, J. D. Blakemore, M. Deimund, H. B. Gray, J. R. Winkler, A. M. Muller, *J. Am. Chem. Soc.* **2014**, *136*, 13118–13121; b) B. M. Hunter, W. Hieringer, J. R. Winkler, H. B. Gray, A. M. Muller, *Energy Environ. Sci.* **2016**, *9*, 1734–1743.  
 [12] Y. Hou, M. R. Lohe, J. Zhang, S. H. Liu, X. D. Zhuang, X. L. Feng, *Energy Environ. Sci.* **2016**, *9*, 478–483.  
 [13] a) M. Gong, Y. Li, H. Wang, Y. Liang, J. Z. Wu, J. Zhou, J. Wang, T. Regier, F. Wei, H. Dai, *J. Am. Chem. Soc.* **2013**, *135*, 8452–8455; b) D. C. Xia, L. Zhou, S. Qiao, Y. L. Zhang, D. Tang, J. Liu, H. Huang, Y. Liu, Z. H. Kang, *Mater. Res. Bull.* **2016**, *74*, 441–446.  
 [14] H. Chen, L. F. Hu, M. Chen, Y. Yan, L. M. Wu, *Adv. Funct. Mater.* **2014**, *24*, 934–942.  
 [15] a) G. Meng, Q. Yang, Y. X. Wang, X. M. Sun, J. F. Liu, *RSC Adv.* **2014**, *4*, 57804–57809; b) Z. Lu, L. Qian, Y. Tian, Y. Li, X. Sun, X. Duan, *Chem. Commun.* **2016**, *52*, 908–911.  
 [16] a) A. N. Mansour, C. A. Melendres, *Surf. Sci. Spectra* **1994**, *3*, 255–262; b) R. D. Smith, M. S. Prevot, R. D. Fagan, S. Trudel, C. P. Berlinguette, *J. Am. Chem. Soc.* **2013**, *135*, 11580–11586; c) J. Qi, W. Zhang, R. Xiang, K. Liu, H. Y. Wang, M. Chen, Y. Han, R. Cao, *Adv. Sci.* **2015**, *2*, 1500199.  
 [17] J. G. Speight, *Lange's handbook of chemistry, Vol. 1*, McGraw-Hill New York, **2005**.  
 [18] B. Zhang, X. Zheng, O. Voznyy, R. Comin, M. Bajdich, M. Garcia-Melchor, L. Han, J. Xu, M. Liu, L. Zheng, F. P. Garcia de Arquer, C. T. Dinh, F. Fan, M. Yuan, E. Yassitepe, N. Chen, T. Regier, P. Liu, Y. Li, P. De Luna, A. Janmohamed, H. L. Xin, H. Yang, A. Vojvodic, E. H. Sargent, *Science* **2016**, *352*, 333–337.  
 [19] M. S. Burke, M. G. Kast, L. Trotochaud, A. M. Smith, S. W. Boettcher, *J. Am. Chem. Soc.* **2015**, *137*, 3638–3648.  
 [20] X. L. Zhu, C. Tang, H. F. Wang, Q. Zhang, C. H. Yang, F. Wei, *J. Mater. Chem. A* **2015**, *3*, 24540–24546.

Manuscript received: May 16, 2017  
 Version of record online: ■ ■ ■ ■ 0000

## ARTICLES

**Keeping it simple:** By immersing nickel foams (NFs) into aqueous solutions containing  $\text{NiCl}_2$  and  $\text{FeCl}_2$  and leaving it to stand for a certain time, microflower-shaped NiFe layered double hydroxides (LDHs) can be generated. The NiFe-LDH/NF electrodes show excellent OER performance with a low overpotential of 210 mV at  $10 \text{ mA cm}^{-2}$  and stable operation for more than 100 charge-discharge cycles in zinc-oxygen batteries.



Z. Yan, E. Wang\*, J. Gao, J. Yang, C. Wu, L. Jiang, M. Zhu, Prof. G. Sun\*

1 – 7

**An Exceptionally Facile Synthesis of Highly Efficient Oxygen Evolution Electrodes for Zinc-Oxygen Batteries**

